Characterizing Twin Structure and Magnetic Domain Structure of Ni-Mn-Ga through Atomic Force

Matthew Reinhold: McNair Scholar

Dr. Peter Müllner: Mentor

Materials Science and Engineering

Abstract

Ni-Mn-Ga is a ferromagnetic shape memory alloy that deforms by twin boundary motion. The magneto-mechanical properties depend strongly on the twin microstructure. A thermomechanical treatment was applied to a Ni-Mn-Ga single crystal with coexisting 10M and 14M martensite structures to create twin boundaries and align the short crystallographic c direction preferentially perpendicular to the surface. The resulting twin structure was characterized using atomic force microscopy (AFM) to obtain the surface relief caused by twinning. Magnetic force microscopy (MFM) was used to find the direction of easy magnetization (which coincides with the crystallographic c direction) of each twin. Among 18 possible twinning histories, ac twinning in 10M martensite was identified as the unique solution. The combination of AFM and MFM after thermomechanical treatment provides a non-destructive characterization of the twin microstructure including the identification of the crystallographic orientation of each twin and of each twin boundary plane.

Introduction

Ni-Mn-Ga is a magnetic shape memory alloy (MSMA) with potential applications in sensor and actuators devices, magnetic refrigeration, power generation, and computer memory. The magnetic, mechanical, and magneto-mechanical properties of Ni-Mn-Ga alloys depend strongly on the composition (e.g., [1,2]), martensite structure (e.g., [3,4]), and twin microstructure (e.g., [5]). Though the martensite structure is controlled to a large extent by the composition, there are compositions around 29-30 at.-% Mn and 20-21 at.-% Ga, for which multiple martensite structures were reported [6,7]. Due to the monoclinic lattice, a variety of twinning modes operate in both 10M and 14M martensites [8,9]. The magnetic-field-induced strain (MFIS) strongly depends on the twin microstructure which can be modified through appropriate training (e.g., [10]). Furthermore, the twin microstructure changes during cyclic experiments, e.g., via actuation in a rotating magnetic field [5,11]. The experimental verification of the correlation between twin microstructure, active twinning modes, and MFIS requires the non-destructive and spatially resolved characterization of twinning modes. It was shown in a recent study that atom probe techniques may be used to solve this task [12]. The aim of the present work is to expand on that study and systematically outline how the combined use of atomic force microscopy (AFM) and magnetic force microscopy (MFM) can be utilized to characterize crystallography and local arrangement of twin variants.

Twinning and Surface Relief

The surface relief at the mesoscopic scale caused by twinning is dependent on martensite orientation and the martensite structure. For monoclinic martensite (10 M and 14M) and surface planes parallel to {100}, the lattice parameters of the unit cell are correlated to the surface relief angle φ_i ($i = a, b, c$) by [12,13]:

$$\varphi_a = \arctan\frac{b}{c} - \arctan\frac{c}{b} \quad (1)$$

$$\varphi_b = \arctan\frac{a}{c} - \arctan\frac{c}{a} \quad (2)$$

$$\varphi_c = \arctan\frac{b}{a} - \arctan\frac{a}{b} \quad (3)$$

where *a*, *b*, and *c* are the lattice parameters when using a pseudo orthorhombic or a pseudo tetragonal unit cell [14][1]. The index *i* of φ_i indicates which crystallographic direction is parallel to the twinning plane. The twinning modes are also named according to the lattice parameters which switch positions across the twin boundary. Fig. 1 shows the example of *ac* twinning with the relief angle φ_b. Table I gives possible φ_i values depending on the type of twinning that occurs and which martensitic variant is present. Values for *a*, *b*, and *c* are taken from Sozinov et al. [3].

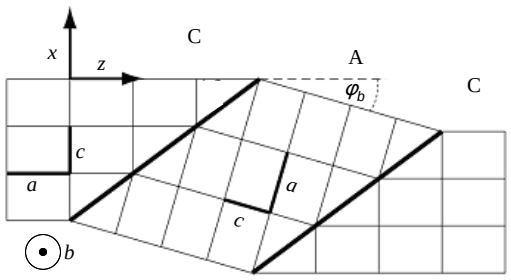

Fig. 1. Schematic illustrating the surface relief produced on a {100} surface by *ac* twinning. This is a cross-section of a twin perpendicular to the *y* direction. The orientation of the orthorhombic unit cell is indicated. The thick black lines are twin boundaries. The twin sequence is CAC (the letters indicate which crystallographic direction is perpendicular to the surface) and the surface relief angle is φ_b.

Table 1. Surface relief angle φ_i values for specific twinning systems in orthorhombic (14M) and tetragonal (10M) martensite calculated with Eqs. 1-3 and using lattice parameter of [3].

Relief Angle	φ_a	φ_b	φ_c
Twinning	*bc*	*ac*	*ab*
Orthorhombic (14M)	2.7°	6.5°	3.7°
Tetragonal (10M)	-	3.5°	-

The surface relief angles listed in Table 1 assume that the twins are formed in a region in which the surface was flat across the entire area prior to the formation of the twin, i.e., in the austenite phase. This is not necessarily the case. Furthermore, the surfaces are assumed to be parallel to {100} planes. To illustrate the variety of possible surface reliefs, a thought experiment is presented here. Assume a surface contains a relief due to *ac* twinning as schematically shown in Fig. 1. Individual twin domains are labeled A and C according to the crystallographic directions *a* and *c*, which are perpendicular to the surface. Now the surface is polished perfectly flat (i.e., the twin relief is removed as in Fig. 2a). Upon heating through the reverse martensitic transformation, the twin boundaries disappear. A surface relief is formed (Fig. 2b) with angles equal and opposite to those in Fig. 1.

In the above thought experiment, the same twinning mode which was present before heating reappears during cooling. These are the only possibilities for twinning in 10M martensite. In 14M martensite, the twinning mode occurring during cooling may differ from the twinning mode present before heating. The next thought experiment explores the combination of different twinning modes using the example of *bc* twinning during cooling. There are again four possibilities. First, for twinning on the previous twinning planes (i.e., inclined to the lower left)

[1] Due to the lattice modulation, the symmetry of the unit cell is actually monoclinic. However, when referring to MFIS, the pseudo orthorhombic and pseudo tetragonal unit cells derived from an orthogonal distortion of the cubic unit cell of the austenite phase are more convenient. Therefore, these unit cells are used throughout this paper; where for convenience, the prefix "pseudo" is dropped.

and a sequence where CAC becomes CBC, the surface relief angle will change by $-\varphi_a$ during cooling so that the final relief angle equals the difference of $\varphi_b - \varphi_a$ (Fig. 4a). Second, the twinning sequence may become BCB and the surface relief angle will change by $+\varphi_a$ during cooling to a total angle of $\varphi_b + \varphi_a$ (Fig. 4b). Third, for twinning on twinning planes inclined to the lower right and a CBC twinning sequence, the surface relief angle will change to a total of $\varphi_b + \varphi_a$ (Fig. 4c). And again the fourth possibility is that the twinning plane orientation may change and the twinning sequence becomes BCB. In this case, the surface relief angle equals the sum of $\varphi_b - \varphi_a$ (Fig. 4d).

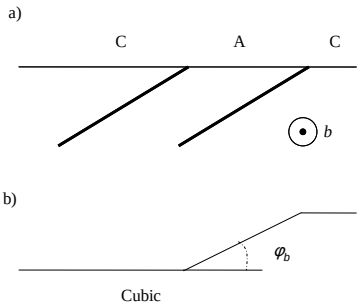

Fig. 2. The *ac* twin found in Fig. 1 (a) after polishing and (b) at a temperature above the martensitic transformation where a double kink appears at the position of the former A domain. The angles are equal and opposite to the angles in Fig. 1.

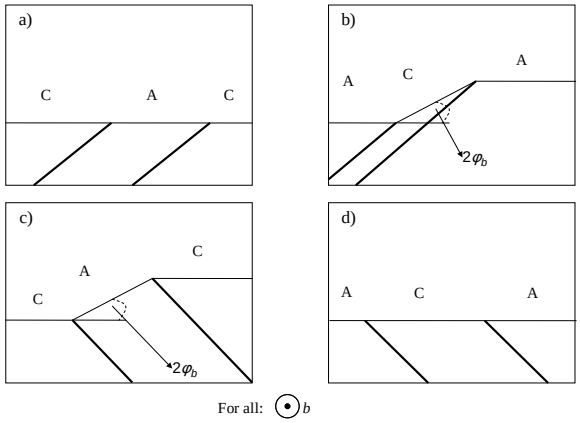

Fig. 3. Twinning options for *ac* twinning when cooling from the situation shown in Fig. 2b. (a) Twinning on the same planes as in Fig. 2a and the same twin sequence ACA changes the relief angle by $-\varphi_b$ and results in a flat surface; (b) reversal of the twin sequence to ACA increases the relief angle by $+\varphi_b$ to a total angle of 2 φ_b; (c) changing the twinning planes also doubles the final relief angle when keeping the sequence CAC; and (d) changing both the twinning sequence (from CAC to ACA) and the twinning plane orientation results in a flat surface.

There are other possibilities upon cooling from Fig. 2b. It is possible that twins will not form and the surface relief angle will be equal to φ_b. Furthermore, all twinning modes may occur with the traces of the twinning planes at different positions. The corresponding relief angles are φ_a, φ_b, and φ_c. Table 2 lists all possible relief angles from starting with one twinning type before thermomechanical treatment and upon cooling with the same type or different type of twinning. The probability of each twinning event depends on extrinsic factors.

Table 2. Total surface relief angle values after polishing going from twinning mode 1 to twinning mode 2 (or vice versa) upon heating and cooling

Structure	**Twinning mode 1**	**Twinning mode 2**	**Relief angle for additive shear [º]**	**Relief angle for subtractive shear [º]**
Tetragonal (10M)	*ac*	*ac*	7.0	0.0
Orthorhombic (14M)	*ab*	*ab*	7.4	0.0
	bc	*bc*	5.4	0.0
	ac	*ac*	13	0.0
	ab	*ac*	10.2	2.8
	bc	*ac*	9.2	3.8
	ab	*bc*	6.4	1.0

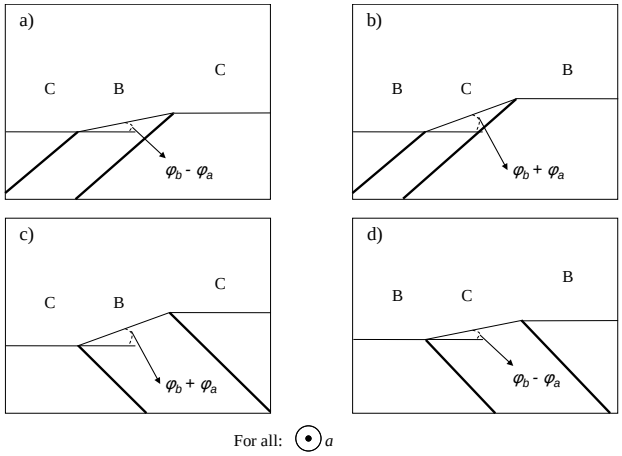

Fig. 4. Twinning options for *bc* twinning upon cooling when starting from the situation shown in Fig. 2b. (a) Twin sequence CBC and the same twin plane orientation as before heating leads to a final surface relief angle of $\varphi_b - \varphi_a$; (b) twin sequence BCB and the same twin plane orientation as before heating leads to a final surface relief angle of $\varphi_b + \varphi_a$; (c) twin sequence CBC with a different twinning plane orientation results in of $\varphi_b + \varphi_a$; and (d) twin sequence BCB with twinning planes inclined to the right results in $\varphi_b - \varphi_a$.

Experimental

A cuboidal sample cut from a $Ni_{50}Mn_{29}Ga_{21}$ (numbers indicate atomic percent) single crystal with faces parallel to {100} was used. Electron diffraction taken on samples from the same crystal revealed two martensite structures, namely 10M and 14M. Cartesian coordinates were defined with the short, mid, and long edges parallel to the *x*, *y*, and *z* directions (Fig. 5). The sample was polished with a 1 μm diamond slurry. The larger face with the *y* direction normal to the surface was finished with Struers OP-AA acidic slurry to a final surface roughness of 2 nm. The sample was then heat treated at 150 °C. During heating and cooling, a constant load of (15 ± 3) MPa was applied in the *x* direction. This was done to align the crystallographic *c* direction parallel to the direction of the applied force. The crystallographic *a* and *b* directions align predominantly and with equal probability parallel to the *y* and *z* directions.

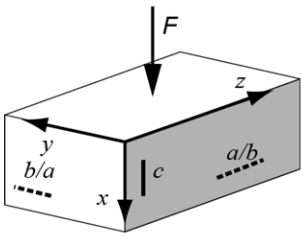

Fig. 5. Loading geometry for the thermomechanical treatment. The sample was compressed parallel to the shortest edge which is the x direction. Cartesian coordinates were defined as indicated. The crystallographic c direction is parallel to the x axis over most of the sample. There are two possibilities for the orientation of the crystallographic a and b directions. The AFM and MFM experiments were performed on the shaded surface normal to the y axis.

A Veeco Dimension 3100 Atomic Force Microscopy System with a Nanoscope V controller was used to characterize the surface relief and the magnetic structure of the surface. The surface relief was imaged in tapping mode using a Veeco MESP ferromagnetic tip coated with CrCo. For MFM, the tip was magnetized so that the magnetic moment of the tip was parallel to the tip axis and perpendicular to the sample surface.

Results

Following thermomechanical treatment, long bands were observed parallel to the *z* direction on the polished surface. These bands were identified as twins. AFM and MFM experiments were performed on the twins. Typical AFM and MFM results are shown in Figs. 6 and 7. The images were taken from the same larger area with a continuous relief of parallel ridges and valleys. Fig. 6a is a 3D height image of several twins and Fig 6b is a 29 μm long cross-section of said twins. The surface relief angle is $\varphi = 3.9° \pm 0.4°$. Fig. 6c and 6d are the 2D height image and 2D magnetic image of the area shown in Fig. 6a.

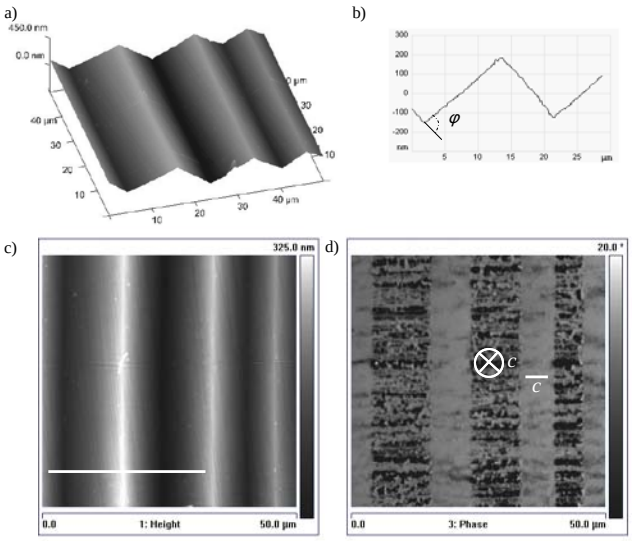

Fig. 6. (a) 3D AFM image of the surface relief found after thermomechanical treatment. The surface relief has bands of positive and negative slope. (b) A 29 μm cross-section of the surface with a surface relief angle $\varphi = 3.9° \pm 0.4°$. (c) AFM height image of the surface relief and (d) MFM magnetic image. The strong contrast indicates out-of-plane magnetization while the weak (neutral) contrast indicates in-plane magnetization [12]. The direction of magnetization is parallel to the crystallographic *c* direction. Every ridge and valley matches with a change in magnetic pattern. The position of the cross-section (b) is marked with a white line in (c).

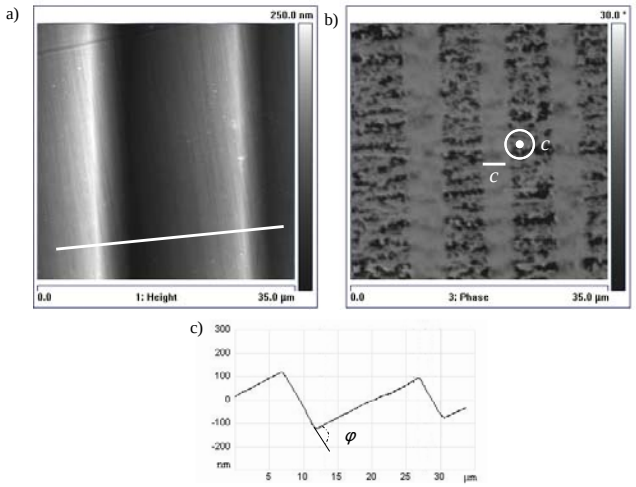

Fig. 7. Second AFM/MFM analysis from an area close to that shown in Fig. 6. (a) AFM height image and (b) MFM magnetic image. There are two ridges (white lines in a) and two valleys (black lines in a). The MFM contains six contrast changes indicating six twin boundaries. (c) A 32 µm long cross-section (position marked in (b) with a white line) yields a surface relief angle $\varphi = 3.7° \pm 0.3°$.

Each change in slope of the surface relief corresponds to a change in the magnetic image of alternating dark and neutral bands. Dark areas in the MFM image indicate that the *c* direction is perpendicular to the surface and the magnetic moment is going into the surface while bright areas correspond to the magnetic moment coming out of the surface [12]. In the bands with soft (or neutral) contrast, the *c* direction is parallel to the sample surface as indicated with a white bar in Fig. 6d.

Fig. 7 shows the AFM 2D height image (Fig. 7a), the MFM image (Fig. 7b), and a 32 µm long cross-section of the height image (Fig. 7c) of a different section of the same larger surface area. For these twins, $\varphi = 3.7° \pm 0.3°$. The AFM and MFM images are similar to what is seen in Fig. 6. However, there is an area in the middle of the scan where no slope change occurs in the surface relief yet there is a change in magnetic contrast from dark to neutral and back to dark. Thus, even though the surface is flat, the magnetization changes from perpendicular to the surface to parallel to the surface and back to perpendicular to the surface. Thus, there are twin boundaries without any surface relief.

Discussion

Since both martensite structures (10M and 14M) are formed in this crystal, all twinning modes with corresponding surface relief angles as listed in Tables I and II may be present. There are 18 twinning histories in total. The values found for the surface relief angle match for single *ac* twinning in 10M martensite and for combined *ac*-*bc* twinning in 14M martensite.

In Fig. 6, each transition from strong contrast to weak (neutral) contrast in the MFM image corresponds to a ridge or valley in the surface relief in the AFM image. The strong contrast in the MFM image shows an alternating of the *c* direction perpendicular and parallel to the surface. If only considering this case, there are four possible twinning histories. If the martensite structure is 10M, the surface relief angle indicates single twinning. Thus, if no twins were present before heating, they must have formed during cooling. If twins were present before heating, the surface relief formed during heating and, therefore, no twinning occurred during cooling. However, the MFM image (Fig. 6d) indicates the presence of twins which rules out the latter case.

If the martensite structure is 14M, the surface relief angle resulted from a combination of *ac* twinning and *bc* twinning. If *ac* twinning was present before heating and *bc* twinning occurred during cooling, then the twin boundaries before and after heat treatment must be inclined towards the lower right (Fig. 8). If on the other hand *bc* twinning was present before heating and *ac* twinning occurred during cooling, then the twin boundaries before and after heat treatment must be inclined towards the lower left. The orientation of the twin boundaries is controlled by

the sequence of twins (e.g., CBC in Fig. 8c) and the position of the C twin domain being on the left side of the ridge (Fig. 6b,c). Analysis of twin crystallography as schematically shown in Fig. 1 yields the orientation of the twin boundary.

At first glance, the AFM and MFM images of the second situation shown in Fig. 7 are very similar to the situation shown in Fig. 6. The difference becomes evident when comparing AFM and MFM images for each case. In the first case (Fig. 6), the magnetic contrast changes six times from strong to weak and back to strong, indicating that there are six vertical twin boundaries in the field of view. Each twin boundary corresponds to a ridge or a valley in the relief which appear as three white lines (for ridges) and three black lines (for valleys) in Fig. 6c. This is in contrast to the situation in Fig. 7. Here again, there are six contrast changes in the magnetic image indicating six twin boundaries. However, the relief image (Fig. 7a) shows only two ridges (white lines) and two valleys (black lines). Therefore, there are two twin boundaries in the center of the image with zero surface relief angles.

As discussed in the thought experiments in the section on twinning and surface relief, a zero surface relief angle can only result when the same twinning mode occurs during cooling as was present before heating. An analysis of all combinations of twinning events yields three histories which are in agreement with the final surface relief and magnetic structure. The first is outlined in fig. 9. Here, there is one A twin domain present before heating. The A domain is sandwiched between two C domains, i.e., the sequence is CAC (Fig. 9a). Upon heating, a double surface kink appears with surface relief angle φ_b (Fig. 9b). Upon cooling, three A domains are formed between C domains, i.e., the final twin sequence is CACACAC. The double surface kink present at high temperature disappears at the position of the central A domain (which was present before heating). Two new surface kinks appear at the positions of the outer A domains with opposite slopes compared to the double kink at high temperature (Fig. 9b). The final situation (Fig. 9c) is in agreement with the experimental findings (Fig. 7) when assuming *ac* twinning in 10M martensite.

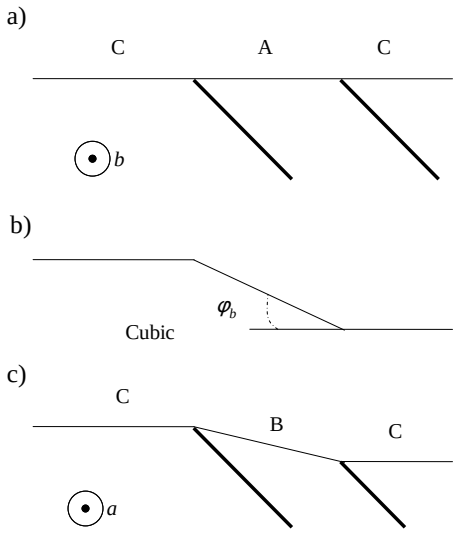

Fig. 8. Possible twinning history for the situation shown in Fig. 6. Before heating (a), there is a CAC twinning sequence without surface kinks (this is the polished surface). (b) The transformation to the cubic austenite phase generates a double kink with surface relief angle φ_b. (c) After cooling, *bc* twinning occurs resulting in a final surface relief angle of φ_b - φ_a.

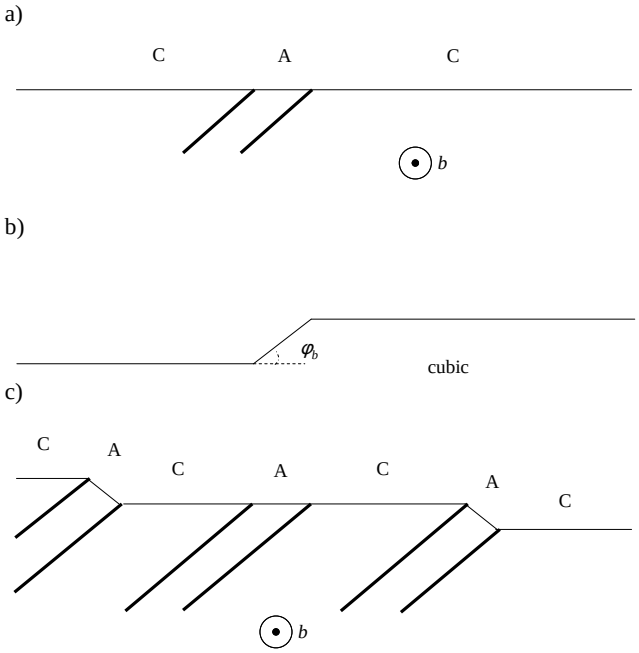

Fig. 9. Possible twinning history for the situation shown in Fig. 7. (a) Polished area with a CAC twin sequence. (b) Upon heating to above the reverse martensitic transformation temperature, a double surface kink with surface relief angle φ_b forms at the position of the former A domain. (c) In the event of *ac* twinning during cooling, the central area forms an *ac* twin with zero surface relief angle while the outer areas form *ac* twins with a surface relief of φ_b.

A number of twinning histories involving a combination of *ac* and *bc* twinning modes, leading to the characterized relief (Figs. 7a,c) and in agreement with the magnetic domain structure (i.e., with the crystallographic c direction out-of-plane where the magnetic contrast is strong, Fig. 7b) may be constructed. As an example, the final (impossible) twin sequence, which might be constructed by starting with a CACACAC twinning sequence (assuming 14M martensite) before heating and assuming CBCACBC twinning sequence upon cooling is shown in Fig. 10. This is in agreement with experiments (Fig.7). However, the direction parallel to the viewing direction is the crystallographic *b* direction in the center twin and the crystallographic *a* direction in the outer twins. Thus, these two twinning systems are not compatible since directions parallel to the twinning planes do not change across a twin boundary. This discrepancy rules out any history with combined *ac* and *bc* twinning.

Hence, the history displayed in Fig. 9 is the only consistent history in agreement with experimental findings. The crystallography of the twinning systems and twin boundary orientations were completely derived from the analysis of the surface relief and the orientation of the magnetic moments as displayed in the MFM images without aid of diffraction methods. These results demonstrate that the combination of atomic force and magnetic force microscopy provides a powerful non- destructive characterization tool for the spatially resolved crystallographic analysis of twinning systems.

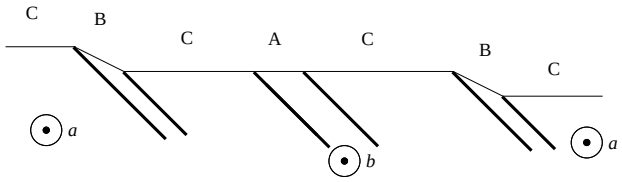

Fig. 10. Impossible twinning sequence for the situation of Fig. 7. The starting sequence is assumed to be CACACAC. After cooling, the central area formed an *ac* twin with a surface relief angle of 0° while the outer areas underwent *bc* twinning leading to a final surface relief angle φ_b - φ_a. The crystallographic direction parallel to the viewing direction is *b* in the center twin domain and *a* in the outer twin domains. This violates compatibility across twin boundaries.

Conclusions

- The surface relief after treatment depends on the presence of twins before polishing and on the twinning mode during cooling.
- The crystallography of twinning systems in Ni-Mn-Ga can be characterized using a combination of AFM and MFM.
- The history of twinning events can be deduced from the analysis of surface relief angles in combination with the magnetic images.

Acknowledgements

The authors thank Linda Kenoyer for assisting in AFM/MFM set-up and Markus Chmielus for assisting with sample preparation. Partial financial support through DARPA contract N66001-01-C-80345, and NIH INBRE P20RR16454 is acknowledged.

References

[1] V. A. Chernenko, E. Cesari, V. V. Kokorin, and I. N. Vitenko (1995). The development of new ferromagnetic shape memory alloys in Ni-Mn-Ga system. *Scripa Mater*, 33, 1239-1244.

[2] V. A. Chernenko (1999). Compositional instability of b-phase in Ni-Mn-Ga alloys. *Scripta Mater*, 40, 523-527.

[3] A. Sozinov, A. A. Likhachev, and K. Ullakko (2002). Crystal structures and magnetic anisotropy properties of Ni-Mn-Ga martensitic phases with giant magnetic-field-induced strain. *IEEE Trans. Magn*,. 38, 2814-2816.

[4] V. A. Chernenko, P. Müllner, M. Wollgarten, J. Pons, and G. Kostorz (2003). Magnetic field induced strains caused by different martensites in Ni-Mn-Ga alloys. *J. Phys. IV France*, 112, 951-954.

[5] M. Chmielus, V.A. Chernenko, W.B. Knowlton, G. Kostorz, and P. Müllner (2008). Training, constraints, and high-cycle magneto-mechanical properties of Ni-Mn-Ga magnetic shape-memory alloys. *Europ. Phys. J. S. T*., 158, 79-85.

[6] M. L. Richard et al. (2006). Crystal structure and transformation behavior of Ni-Mn-Ga martensites. *Scripta. Mater*., 54, 1797-1801.

[7] M. L. Richard et al. (2007). Martensite transformation in Ni-Mn-Ga ferromagnetic shape-memory alloys. *Metall. Mater. Trans. A*, 38, 777-780.

[8] P. Müllner, D. Mukherji, M. Aguirre, R. Erni, G. Kostorz (2005). Micromechanics of magnetic-field-induced twin-boundary motion in Ni-Mn-Ga magnetic shape-memory alloys. Proc. 'Solid-to-solid phase transformations in inorganic materials 2005' (PTM'05), Vol. 2, (TMS, Warrendale, PA), p. 171-185.

[9] M. Han, F. F. Kong (2008). Twin boundary structure of the modulated variants in a Ni-Mn-Ga alloy. *J. Alloys Comp.*, 458, 218-222.

[10] S. J. Murray, M. Marioni, S. M. Allen, R. C. O'Handley, and T. A. Lograsso (2000). 6% magnetic-field-induced strain by twin-boundary motion in ferromagnetic Ni-Mn-Ga. *Appl. Phys. Lett*., 77, 886-888.

[11] P. Müllner, V. A. Chernenko, and G. Kostorz (2004). Large magnetic-field-induced deformation and magneto-mechanical fatigue of ferromagnetic Ni-Mn-Ga martensites. *Mater. Sci. Eng. A*, 387-389, 965-968.

[12] P. Müllner, Z. Clark, L. Kenoyer, W. B. Knowlton, and G. Kostorz (2008). Nano-mechanics and magnetic structure of orthorhombic Ni-Mn-Ga martensite. *Mater. Sci. Eng. A*, 481-482, 66-72.

[13] N. Lanska and K. Ullakko (2003). Microstructure change in Ni-Mn-Ga seven-layered martensite connected with MSM effect. *J. Phys. IV France*, 112, 925-928.

[14] Y. Ge et al. (2003). Crystal structure of three Ni-Mn-Ga alloys in powder and bulk materials. *J. Phys. IV France*, 112, 921-924.